

1 **Nano-Fluidic Traps by Two-Photon Fabrication for**
2 **Extended Detection of Single Macromolecules and Colloids**
3 **in Solution**

4
5 **Oliver Vanderpoorten^{1,2,3,4,+}, Ali Nawaz Babar^{1,3+}, Georg Krainer^{1,+}, Raphaël P.B. Jacquat^{1,+}, Pavan K.**
6 **Challa¹, Quentin Peter¹, Zenon Toprakcioglu¹, Catherine K. Xu¹, Ulrich F. Keyser³, Jeremy J. Baumberg³,**
7 **Clemens F. Kaminski², and Tuomas P. J. Knowles^{1,3*}**

8
9 ¹Yusuf Hamied Department of Chemistry, University of Cambridge, Lensfield Road, Cambridge, CB2 1EW, UK

10
11 ²Department of Chemical Engineering and Biotechnology, University of Cambridge, Philippa Fawcett Drive,
12 Cambridge, CB3 0AS, UK

13
14 ³Cavendish Laboratory, Department of Physics, University of Cambridge, J. J. Thomson Avenue, Cambridge,
15 CB30HE, UK

16
17 ⁴Department of Physics and Technology, UiT The Arctic University of Norway, Tromsø, NO-9019, Norway

18
19 *To whom correspondence should be addressed: tpjk2@cam.ac.uk

20
21 ⁺These authors contributed equally to this work.

22
23 Keywords: Nanoparticle trapping, Nanofluidics, 2-photon lithography, Protein oligomers, DNA, Molecular
24 trapping, Confocal fluorescence detection, Soft lithography

25 **Abstract**

26
27 The analysis of nanoscopic species, such as proteins and colloidal assemblies, at the single-molecule level has
28 become vital in many areas of fundamental and applied research. Approaches to increase the detection timescales
29 for single molecules in solution without immobilising them onto a substrate surface and applying external fields
30 are much sought after. Here we present an easy-to-implement and versatile nanofluidics-based approach that
31 enables increased observational-timescale analysis of nanoscopic material building blocks such as single
32 biomacromolecules and nanoscale colloids in solution. We use two-photon-based hybrid lithography in
33 conjunction with soft lithography to fabricate nanofluidic devices with nano-trapping geometries down to 100 nm
34 in height. We provide a rigorous description and characterisation of the fabrication route that enables the writing
35 of nanoscopic 3D structures directly in photoresist and allows for the integration of nano-trapping and nano-
36 channel geometries within micro-channel devices. Using confocal fluorescence burst detection, we validated the
37 functionality of particle confinement in our nano-trap geometries through measurement of particle residence times.
38 All species under study, including nanoscale colloids, α -synuclein oligomers, and double-stranded DNA, showed
39 a three to five-fold increase in average residence time in the detection volume of nano-traps, due to the additional
40 local steric confinement, in comparison to free space diffusion in a nearby micro-channel. Our approach thus
41 opens-up the possibility for single-molecule studies at prolonged observational timescales to analyse and detect
42 functionalized nanoparticles and protein assemblies in solution without the need for surface immobilisation.

43 **Introduction**

44
45 The spatial confinement of biomolecules or colloidal nanoparticles in solution for biophysical studies at the single-
46 molecule level has become instrumental in many areas of fundamental and applied research including
47 nanobiotechnology [1], biophysics [2], and clinical diagnostics [3]. It allows for increased observational-timescale
48 analysis of nanoscopic species such as nucleic acids, protein assemblies [4] or colloidal particles [5] with single-
49 molecule sensitivity [6]. Improved nanoscopic single-molecule detection schemes are key for the development of
50 new material building blocks on the nanoscale, which play an essential role in bottom-up assembly processes of
51 meta materials [7], amyloid fibrils [8] and DNA origami technology [9], as well as in nanoparticle synthesis and
52 their surface functionalization [10]. Currently, molecular confinement is most typically achieved through surface
53 immobilisation of the biomolecule or nanoparticle of interest on a substrate surface (e.g., for confocal or total
54 internal reflection fluorescence (TIRF) microscopy) [11],[12],[13]. This approach, however, has numerous
55 drawbacks, not least because surface interactions can change the molecule's configuration and function.
56

57 An alternative to surface immobilisation is the trapping of particles in solution without immobilising them onto a
58 substrate surface. Various approaches using external fields, such as electric [14], hydrodynamic [15] and optical
59 fields [16], [17], for nanoparticle trapping in solution have emerged. Optical trapping, for example, has proven
60 effective in measuring repulsive or attractive forces between particles such as colloids and proteins, but the high
61 laser powers required induce flows around the trapped particles leading to undesirable and confounding effects
62 [1]. Furthermore, such techniques suffer from low throughput and require a refractive index mismatch between
63 the particle and its surrounding media [18], which is often not the case when monitoring biological specimens.
64 Other techniques, such as thermal trapping [19]–[21], have also shown to be effective at confining nanoparticles
65 in small volumes, but similar to optical trapping, thermal particle trapping has significant drawbacks due to the
66 sample undergoing motion because of convection. This puts limitations on the estimation of particle properties
67 such as molecular size and particle reaction kinetics at physiologically relevant conditions.
68

69 Recently, geometry-induced electrostatic trapping and colloidal trapping based on the spatial modulation of
70 configurational entropy was demonstrated [22],[23]. This approach enables trapping without applying external
71 fields and has proven invaluable in observing particles in an all aqueous environment [24]. Mojarrad et al. [25]
72 demonstrated trapping of colloids and gold nanoparticles in nanofluidic silica devices, which allowed
73 measurement of their particle size and charge in silica-based nano-wells. Ruggeri et al. [26],[27] further pushed
74 the limits of nano-trapping-based electrometry to the single-molecule level. While efficient in their use, however,
75 to date, the fabrication of such trapping devices and their subsequent integration with microfluidic device platforms
76 is challenging and demands specialised clean room equipment such as electron beam lithography (EBL) [28] and
77 reactive ion etching (RIE) [29]. Even though such approaches generate nano-slits or nano-channels smaller than
78 100 nm [30], the complexity of the fabrication process, writing times, and the costs to produce a single device
79 render these techniques highly inefficient and impractical. Additionally, most of these techniques are relatively
80 low throughput and integrating them with micro-channels, which is required for the chip-to-world interface, can
81 be challenging.
82

83 An alternative approach for fabricating nano-traps/nano-channels and integrating the nanostructures within a
84 microfluidic chip platform involves the combination of conventional UV lithography followed by two-photon
85 lithography (2PL) [31],[32], where a focused femto-second pulsed laser is scanned across the photoresist, resulting
86 in the writing of device features below 200 nm in lateral size. 2PL or direct laser writing (DLW) is a powerful
87 emerging technology and has gained much attention in the last years for the fabrication of 3-dimensional (3D)
88 micro- and nano-structures and functional devices below the diffraction limit [33]. Fabrication of arbitrary 3D
89 structures is possible in a photoresist from computer-generated 3D models and thus constitutes a fast and
90 straightforward fabrication procedure [34]. Previously, microfluidic [35], nanofluidic [36], and optofluidic [37]
91 devices were fabricated using femto-second laser 3D micromachining and were shown to allow for the integration
92 of functionalities unachievable with conventional UV-lithography in device designs.
93

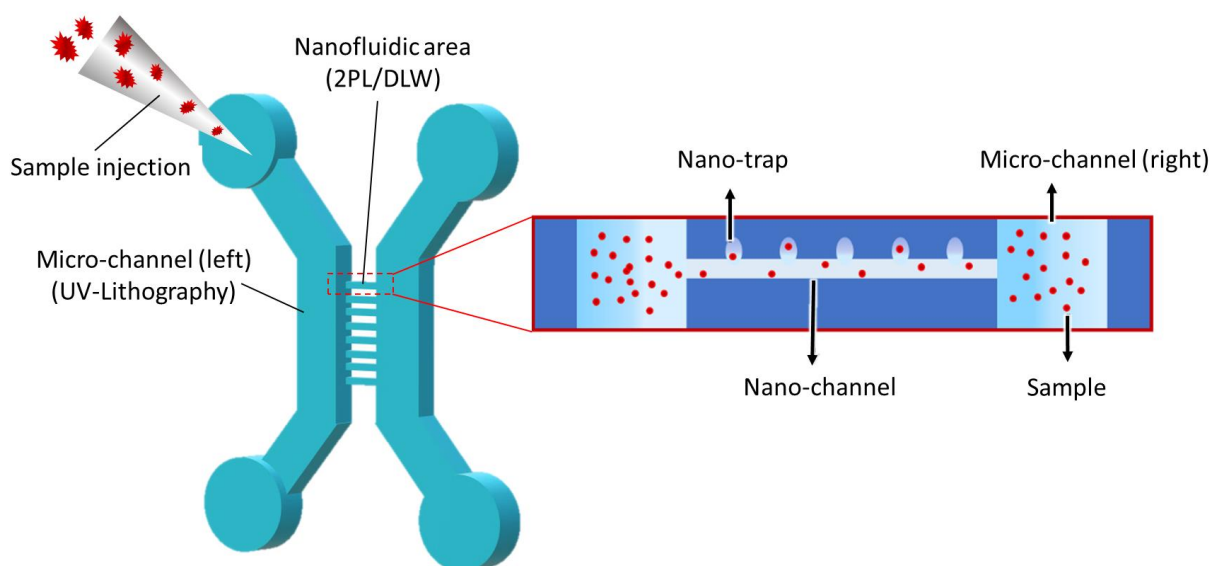
94 Here, we demonstrate the facile fabrication of nanofluidic trapping devices using a 2PL system for increased
95 observational-timescale single-molecule studies of biomacromolecules and colloids in solution. To this end, we

96 developed an approach based on hybrid 2PL- and UV-lithography in conjunction with soft lithography [38] to
 97 generate nanoscale channels and adjacent nanoscale trap structures with dimensions down to 100 nm in height in
 98 a single step from a silicon master wafer. This allowed for the fabrication and prototyping of nanofluidic
 99 polydimethylsiloxane (PDMS)-silica devices in a facile and scalable manner and the writing of various nano-
 100 trapping geometry designs with varying heights in one writing process. We analysed the master wafer and PDMS
 101 imprints using correlative scanning electron microscope (SEM) and atomic force microscope (AFM)
 102 characterisation techniques and validated the functionality of particle confinement in nano-trap geometries through
 103 measurement of particle residence times in nano-traps as compared to micro-channels and nano-channels using
 104 single-molecule fluorescence burst analysis. We found that all species analysed, including nanoscale colloids,
 105 protein oligomers, and short DNA duplexes, showed a three- to five-fold increase in average residence time in the
 106 detection volume of nano-traps in comparison to free space diffusion in a nearby nano- or micro-channel. We
 107 further demonstrate other fluorescence microscopy techniques (confocal imaging and TIRF microscopy) as
 108 alternative readout techniques to be used in combination with nanofluidic traps. Taken together, our developments
 109 presented herein constitute a cost-effective and easy-to-implement approach for the fabrication of nanofluidic trap
 110 devices and open-up a broad avenue of possibilities to study single molecules in solution for extended periods of
 111 time without permanent surface immobilization and without applying external fields.

112 Results and Discussion

113 Integration of nano-trapping and nano-channel geometries between micro-channels with 2-photon 114 lithography

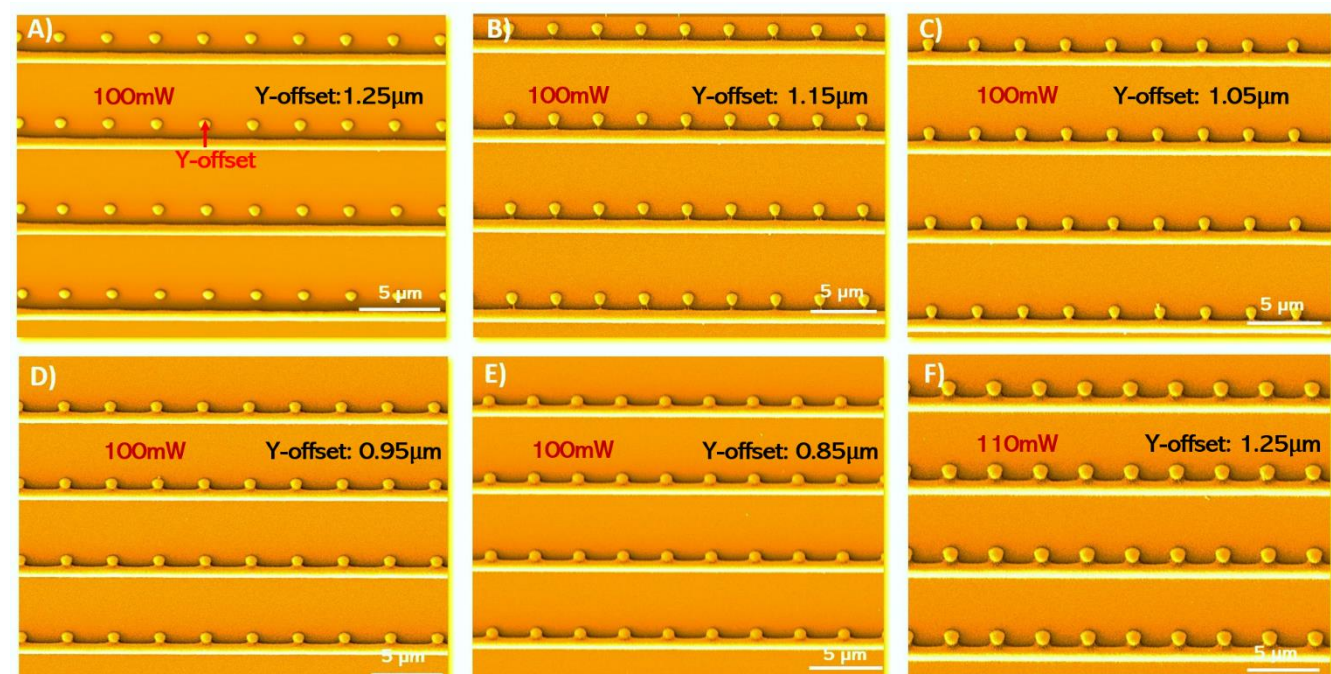
115 Conventional fabrication of trapping devices relies on sophisticated clean-room equipment [22] and does not allow
 116 high throughput and flexibility in the writing of structures of varying geometry and height. To overcome these
 117 challenges and make the fabrication process more facile, we propose here a fabrication route of nanofluidic devices
 118 via hybrid 2PL that enables the writing of nanoscopic 3D structures directly in photoresist [32]. By combining
 119 large area UV mask lithography with local high precision two-photon laser writing, we demonstrate the integration
 120 of nano-traps written adjacent to nano-channels in a pre-existing microfluidic device design (see **Figure 1**). Since
 121 2PL is a dosage-dependent process and the smallest feature size obtained in the photoresist depends on the laser
 122 intensity and exposure time, we first set out to first optimise the fabrication procedure to achieve full merging of
 123 nano-trap and nano-channel geometries.



128 **Figure 1. Design and fabrication of nanofluidic device with trapping functionalities.** Schematic of the device design
 129 consisting of microfluidic reservoirs, inlets/outlets, nanofluidic channels and nano-trapping arrays. 2-photon lithography
 130 (2PL) (or direct laser writing, DLW) is used to combine microfluidics with nanofluidic functionalities. Large area mask-based
 131

132 UV lithography patterns microfluidic areas, whereas 2PL incorporates nano-channels and nano-traps in between two micro-
133 channels. The inset illustrates the placement of the nano-traps next to the nanofluidic channel.

134
135 We began by exploring and prototyping nanofluidic geometries in negative SU-8 photoresist (**Figure 2**) and
136 produced imprints into PDMS following standard UV- and soft-lithography protocols (**Figure 3**). Characterization
137 techniques such as SEM and AFM were used to analyse the prototype nanostructures. Varying the laser power,
138 laser writing speed, and the distance in between the nano-traps and nano-channel (Y-offset) during the 2PL writing
139 process resulted in different configurations of nano-trap moulds as shown in **Figure 2 (A–E)**. Straight nano-
140 channels were written at a fixed laser intensity of 90 mW and a writing speed of 100 $\mu\text{m}/\text{s}$. Dots for nano-trap
141 moulds were written adjacently with 1000 $\mu\text{m}/\text{s}$ scanning speed and by modulating the laser at 100 mW. Nano-
142 traps were added every 3 μm along the nano-channels. The height of the nano-traps was smaller than the nano-
143 channels due to the lower net exposure of the photoresist. Notably, the 3D piezo-flexure stage used for scanning
144 of the laser beam is a key component and allowed for varying the Y-offset between nano-traps and nano-channels
145 with a resolution down to 10 nm by leveraging the closed-loop control mode of a piezo stage. Accordingly, the Y-
146 offset was varied from 1.25 μm to 0.85 μm in steps of 100 nm. As shown in **Figure 2 (B)**, at a Y-offset of 1.15
147 μm , the SU-8 of the nano-trap geometry merged with the nano-channel through monomer cross-linking. The same
148 geometries were also analysed in the PDMS imprints as shown in SEM micrographs of **Figure 3 (A–E)**. Notably,
149 by just varying the Y-offset between the nano-channel and nano-traps, different geometries and designs of the
150 nano-traps in PDMS could be generated, for example, triangular nano-traps as shown in **Figure 3 (B)**. This
151 highlights the importance of precise laser positioning to control not only the merging of nano-channels with nano-
152 traps, but also the possibility to create traps with varying geometries. The process of 2PL for writing almost
153 arbitrary 3D structures thus allows significant flexibility here for choosing and modulating the desired geometry,
154 microfluidic chip design, and introducing multiple geometry layers within a single spin-coating process. Indeed,
155 we were able to add other conformations of traps to a nano-channel, for example, where the traps were positioned
156 on top of the nano-channels (**Figure 3 (G)**) or nano-traps with bottle-neck openings (**Figure 3 (H)**) on the side.
157 The latter structures exhibited a nano-trap height of 100 nm, as confirmed by correlative SEM/AFM measurements
158 on the master wafer (**S1**).



160
161 **Figure 2. Prototypes of nano-channel and nano-trap geometries fabricated in photoresist using 2-photon lithography.**
162 Shown are SEM micrographs of nano-channel/nano-trap moulds as obtained by 2-photon lithography in SU-8 photoresist
163 using varying laser powers and Y-offsets. The writing speeds for the nano-traps and nano-channels were 1000 $\mu\text{m}/\text{s}$ and 100
164 $\mu\text{m}/\text{s}$, respectively. (A)–(E) Nano-channel/nano-trap moulds obtained with a Y-offset in the range of 1.25–0.85 μm ; the laser
165 power for writing nano-channels and nano-traps was 90 mW and 100 mW, respectively. (F) Optimized nano-channel/nano-

trap mould written with a Y-offset of 1.25 μm ; the laser power for writing nano-channels and nano-traps was 100 mW and 110 mW, respectively.

The prototyping geometries obtained thus far were used to determine appropriate and optimised writing parameters for creating nanofluidic trapping devices required for nanoparticle and biomolecule trapping in single-molecule experiments (see below). For this chip design, we required round nano-trapping cavities of a few hundred nanometres in radius which are well-merged with straight nano-channels that have dimensions in the submicron-regime. Such geometrical features could be obtained by using 110 mW laser power for writing of the traps, 100 mW for the nano-channels and a Y-offset in between them of 1.25 μm (**Figure 2 (F)**). Thereby, we fabricated nano-traps of 350 nm in radius adjacent to nano-channels of 650 nm in width. The chosen fabrication parameters show geometrical consistency between individual traps and are still mechanically stable enough to have the same structures in the final bonded device. The mechanical stability of the nano-trap structures in SU-8 was further enhanced by increasing the cross-linking density of monomers with a second UV exposure after writing nanostructures with 2PL [39].

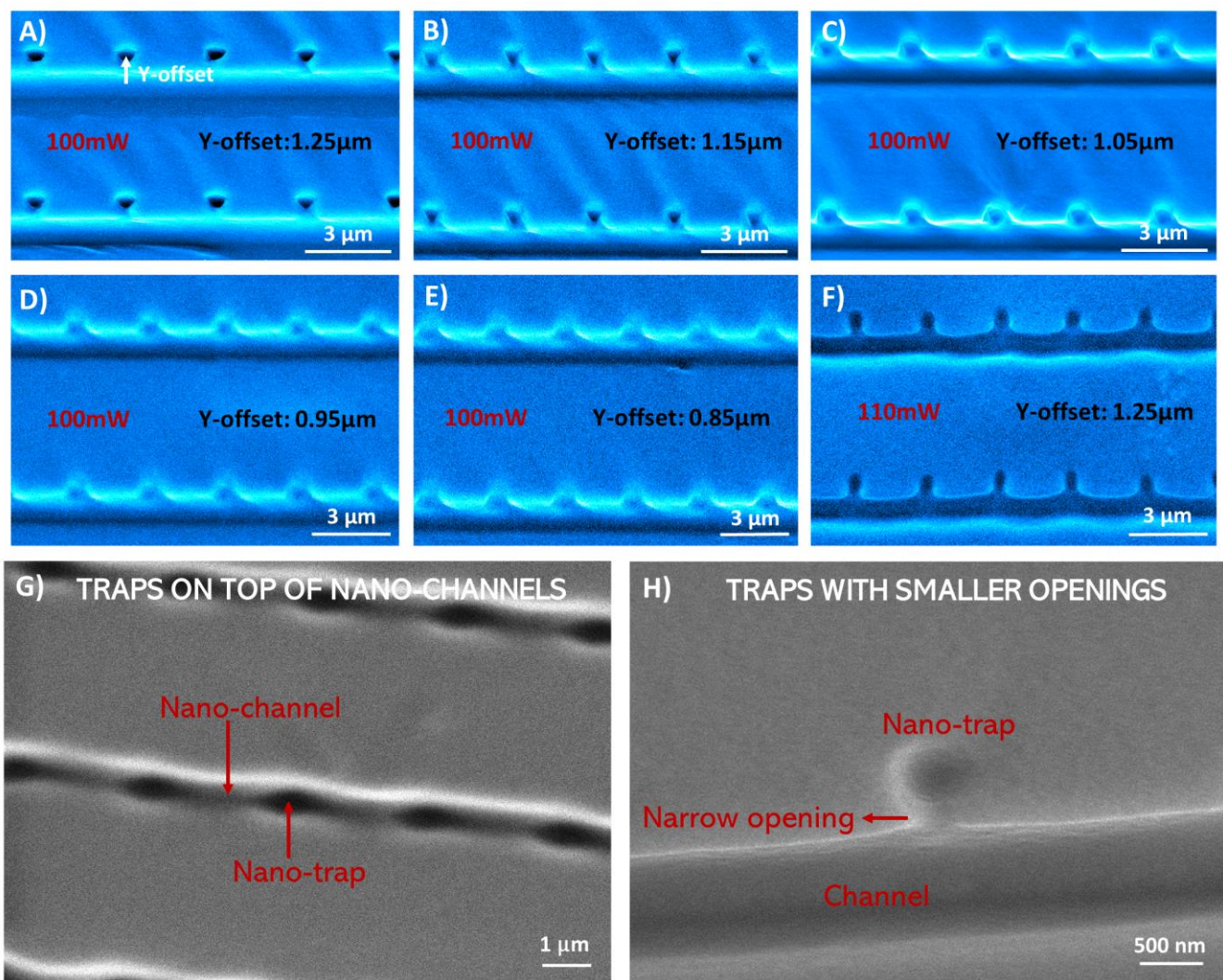
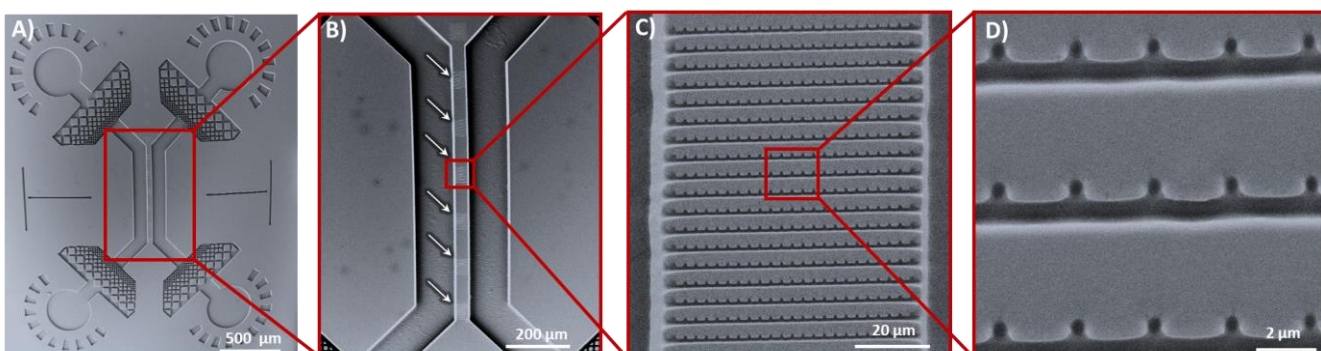


Figure 3. PDMS imprints of nano-channel and nano-trap device prototypes. Shown are SEM micrographs for nano-channels and nano-traps imprinted in PDMS. The moulds, from which the PDMS imprints were fabricated, were written in SU-8 photoresist with 2PL by varying the laser power and Y-offset (Figure 2). The writing speeds for the nano-traps and nano-channels were 1000 $\mu\text{m}/\text{s}$ and 100 $\mu\text{m}/\text{s}$, respectively. (A)–(E) Nano-channels and nano-traps imprinted in PDMS with Y-offset in the range from of 1.25 μm –0.85 μm ; the laser power for nano-channels and nano-traps were 90 mW and 100 mW, respectively. (F) Optimized nano-channel/nano-traps imprinted in PDMS with Y-offset of 1.25 μm ; the laser power for nano-channels and nano-traps were 100 mW and 110 mW, respectively. (G) SEM image of a trapping device with nano-traps on

189 top of nano-channels in the PDMS (top view). (H) SEM image of the narrow opening of a nano-trap imprinted in PDMS.
190 Correlative AFM imaging showed a height of approx. 100 nm of the pockets (**S1**).
191

192 Integration of nano-channel and nano-trap geometries in a microfluidic device platform

194 After having optimised the procedures for generating nano-trap and nano-channel geometries via our 2PL
195 approach, we set out to fabricate the combined nanofluidic device for single-molecule experiments, as shown in
196 **Figure 1**. The device was produced by first generating the micron-scale structures of the chip, which consisted of
197 two microfluidic channels and reservoirs, sample inlets/outlets and pre-filters. This was done by transferring these
198 chip features from a high-resolution transparency acetate photomask onto SU-8 photoresist, spin-coated on a
199 silicon wafer, via conventional contact UV lithography [30]. In a second step, the microfluidic channel reservoirs,
200 separated by 75 μm , were connected with straight nano-channels and adjacent nano-traps using the optimised 2PL
201 writing parameters, as detailed above (c.f., **Figure 2 (F)** and **Figure 3 (F)**). Subsequently, PDMS imprints and
202 glass-bonded chips were produced from these structures using standard soft lithography and replica moulding
203 procedures. **Figure 4 (A)** shows a SEM micrograph of the final PDMS imprint with an overview of the
204 conventional micron-scale chip functionalities. Further magnification (**Figure 4 (B)–(D)**) shows the successful
205 integration of nanofluidic functionalities in between the microfluidic reservoirs. Two microfluidic compartments
206 of 25 μm depth were joined by 2PL with six nanofluidic areas (**Figure 4 (B)**, indicated with arrows). **Figure 4 (C)**
207 shows in greater detail one nano-trapping array consisting of 18 nano-channels with adjacently added nano-traps
208 every 3 μm . Notably, the channels show a wider funnel-like shape at the microfluidic interface due to the sequential
209 double exposure of the photoresist by UV-lithography and 2PL. The central part of the array, however, shows the
210 intended trap geometry from the prototypic procedure above, with suitable traps for confinement of nanoparticles
211 imprinted in PDMS. The nano-channels were 650 nm wide and connected to the nano-traps, which had a radius of
212 350 nm. The nano-channels and nano-traps were 750 nm and 650 nm in height, respectively, according to
213 correlative profilometer measurements (**S2**).
214



215
216 **Figure 4. Nanofluidic device with trapping functionalities for single-molecule experiments.** Shown are SEM micrographs
217 of PDMS nanofluidic device imprints fabricated via hybrid UV mask lithography and 2PL. (A) Full view of the micro-
218 /nanofluidic device, consisting of microfluidic reservoirs, inlets/outlets, nanofluidic channels and nano-trapping arrays. The
219 design corresponds to the schematic shown in Figure 1. (B) Magnification depicting the arrays of 75 μm long nano-channels
220 with integrated nano-traps in between the two 25 μm deep micro-channels in PDMS. (C) Higher magnification of nanofluidic
221 channels and nano-traps shows consistent imprinting of nano-trapping arrays in PDMS. (D) Zoom-in of SEM micrograph
222 showing the geometry of nano-traps.
223

224 Single-molecule fluorescence detection of colloids and biomolecules in nano-traps

225 Single-molecule studies for biological measurements in miniaturised devices have proven very useful due to their
226 precise sample handling, small volume manipulation, and high throughput capabilities [40], [41]. Prolonged
227 observation of single molecules or nano-colloids in solution is still a challenging task but an important step towards
228 microfluidic total-analysis systems (μTAS). [42] Our chip design provides an opportunity for prolonged detection
229 of single particles in solution without permanent surface immobilization. We intend to increase particle residence
230 times in a detection volume due to the additional local steric confinement in the nano-traps.
231

To demonstrate this, we set out confocal-based single-molecule burst experiments that allowed us to observe, record, and compare the events of single particles entering and leaving the nano-trapping geometry. **Figure 5** schematically illustrates the experimental setup. The device's micro-channel reservoirs were filled with respective particle solutions at pico- to nano-molar concentrations. Once the sample in the device reached equilibrium and the nanoparticles started diffusing through the nano-channels, fluorescence burst detection was conducted within the nano-traps. Samples were excited with a continuous 488-nm diode laser and their fluorescence collected using avalanche photodiodes, which allowed readout of the fluorescent nanoparticle signal with high temporal resolution.

We first performed measurements on 40 nm fluorescent particles and compared burst detection under nano-trap confinement to residence times in the microfluidic reservoirs of the device and the nano-channel bridges. To this end, the confocal detection volume was placed in the respective region of the device, as illustrated in **Figure 5** (A)–(C). Within the microfluidic part of the device (**Figure 5** (A)), multiple fluorescence burst signals are overlapping during the measurement and show various intensity levels, due to multiple particles being able to cross through the detection volume at the same time. The time regime of transition events is in the millisecond range. In a second measurement, the laser spot was placed inside a nano-channel, as shown in **Figure 5** (B), and confocal time traces were recorded. The number of fluorescence bursts was drastically reduced due to the single-molecule exclusion capabilities of the nano-channel, and just slightly increased detection times in comparison to measurements in the microfluidic channel were observed. Finally, we placed the confocal spot at the centre of a nano-trap. Nanoparticles in a single nano-trap geometry were recorded as shown in **Figure 5** (C). The time trace shown exemplifies the prolonged nature of fluorescence burst signals obtained within a nano-trap and is common amongst all species under study (S3).

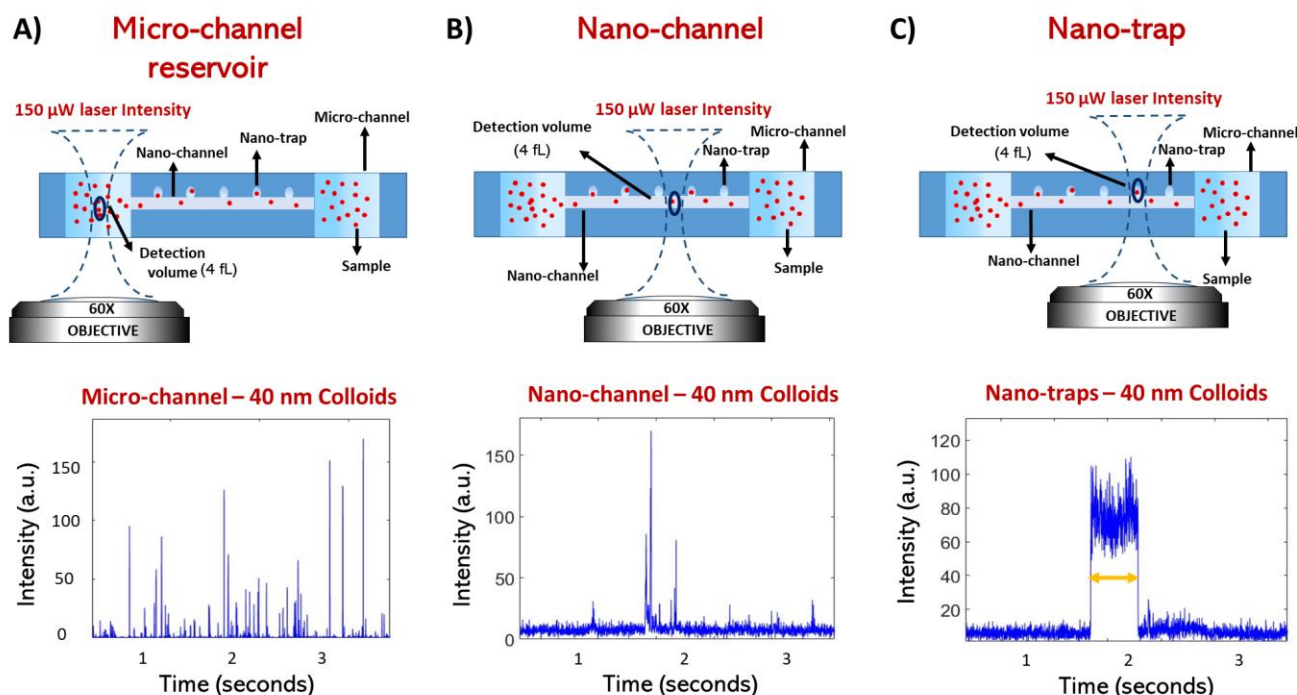


Figure 5. Single-molecule fluorescence detection in microfluidic reservoirs, nano-channels regions and under nano-trap confinement. (A) The confocal detection volume was placed into the microfluidic part of the device at the mid height of the channel (i.e., 13 μm above the glass cover slip). The diffusion of multiple particles at the same time through the confocal spot results in multiple fluorescence bursts as shown in the fluorescence burst time trace. (B) The confocal fluorescence burst detection volume was placed in the nano-channel region. Fluorescence data recorded in the nano-channel shows more rare events of fluorescent bursts, which implies that the probability of multiple particles crossing the detection volume is lowered by the nano-channel confinement. (C) The detection volume was placed into the centre of a nano-trap geometry. The fluorescence time trace data shows significantly increased residence time of single particles up to ten to hundreds of milliseconds under nano-trap confinement.

Using the same nanofluidic geometry, we compared the behaviour of differently sized particles in the nano-traps. We performed experiments, as described before, with a series of nano-colloids and biomacromolecules, including 100 nm colloids, 40 nm colloids, α -synuclein oligomers ($\sim 9-14$ nm), and 45 bp DNA (~ 15.3 nm length, estimated with 0.34 nm per bp, rod-like) [43][44] in deionized water. Our results show that the nano-traps increase the residence time of particles within the detection volume due to the additional local steric confinement. **Figure 6** shows a comparison of their mean residence times inside the nano-traps in relation to microfluidic channels. The time spent by the particle inside the laser spot depends on its diffusional properties and therefore on its size. In general, according to the Stokes-Einstein relation, the diffusion coefficient is defined as $D = (k_B T)/(6\pi\eta R_H)$, where R_H is the hydrodynamic radius, k_B the Boltzmann constant, T the temperature and η the viscosity. This trend can be observed for confined and non-confined particles. Strikingly, comparing the nano-trap residence time to the microfluidic channel indicates an up to 5-fold increase of observation time within the confocal detection volume. This is expected because the walls limit the possibility of the molecule escaping from the laser's field of view, as mentioned above. The Debye length can be assumed to be less than 100 nm [45] and should not be the major factor in the confinement presented here, but definitely needs to be considered when using smaller nanofluidic design dimensions instead. Enhancement of the residence time, once the particle is in the nano-trap, thus enables longer signal capture of a single particle. This opens-up the possibility for single-molecule metrology of biomolecules and colloids in solution over extended periods of time.

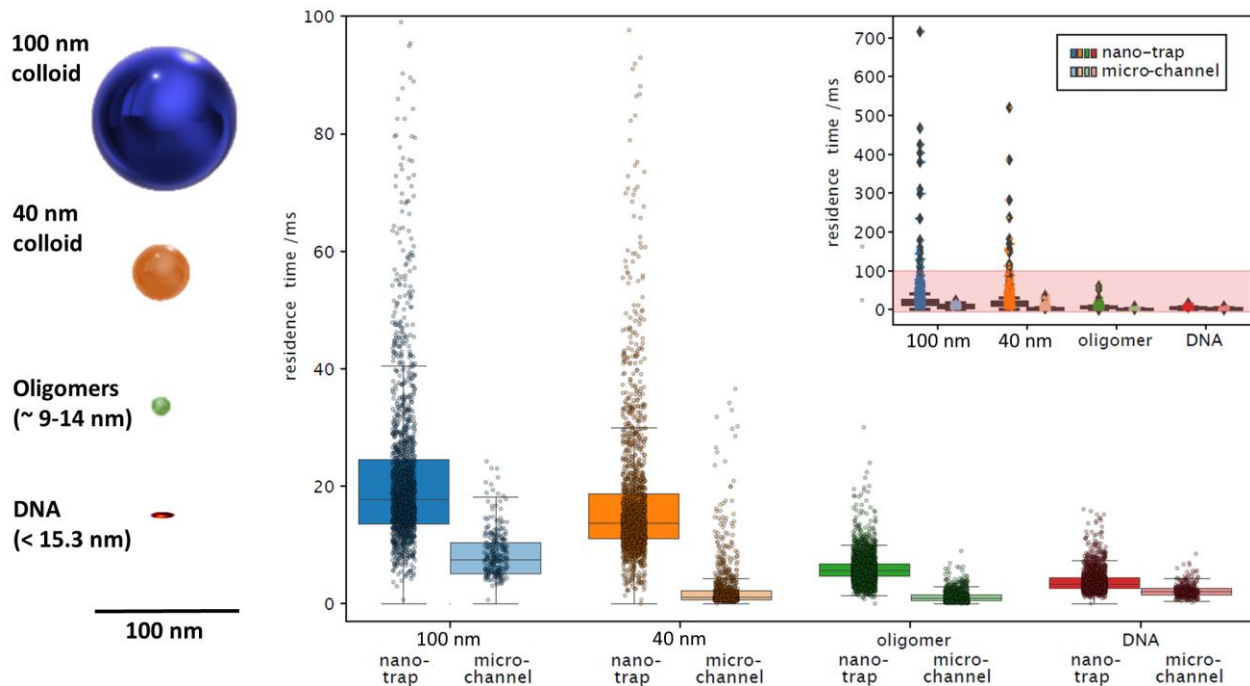


Figure 6. Residence time of specimen under nano-trap confinement. (A) Schematic illustration of the relative size difference of specimen probed. (B) Comparison between residence times for 100 nm colloids, 40 nm colloids, α -synuclein oligomers, and 45 bp DNA in micro-channel reservoirs and nano-trapping geometries. Residence time in nano-traps relative to the detection time in micro-channel reservoirs is increased by a factor of approximately 3- to 5-fold. The insert shows the existence of rare trapping events in the hundreds of millisecond range for colloidal particles, and up to tens of millisecond for oligomers and DNA.

Conclusions

In this paper, we have demonstrated the use of hybrid 2PL for the fabrication of nano-traps written adjacent to nanofluidic and microfluidic channels and their usage for the study of colloidal nanoparticles and biomacromolecules at the single-molecule level. We have established conditions for the successful generation of a silicon master wafer with nanoconfinement geometries in a negative SU-8 photoresist by combining 2-photon direct laser writing with UV lithography. We imprinted nanofluidic devices from the silicon master wafer into PDMS to make functional nano-channels with adjacent nano-traps of 350 nm radius and 650 nm height, but also

301 much smaller geometries, and structures below 100 nm in height, are possible (**S1**). Given the ease of fabrication,
302 our approach can be readily adopted by laboratories with access to commercial or custom-built 2PL systems and
303 allows for the fabrication and prototyping in a high-throughput and scalable manner as opposed to EBL and
304 sequential clean room nanofabrication techniques.

305
306 To demonstrate the applicability of the nano-trapping devices developed herein for prolonged observation of single
307 molecules, we used single-particle fluorescence burst detection to measure the residence time of polymer
308 nanoparticles such as 100 nm and 40 nm colloids, and various biological relevant samples like α -synuclein
309 oligomers and fluorescently labelled 45 bp DNA in nanofluidic confinement. Although our nano-trap geometry is
310 orders of magnitude larger in comparison to the biological specimen under study, we observed a significant
311 increase in residence times of the samples. All species analysed in the same trapping geometry showed up to 3- or
312 5-fold increase of observation time in a diffraction limited confocal detection volume. This finding is significant,
313 as it opens-up the possibility to study and analyse biomacromolecules or biomolecular assemblies in solution
314 without permanent surface immobilization for extended periods of time. It also allows longer observation of the
315 same molecule for optical techniques that greatly benefit from higher photon counts such as Förster resonance
316 energy transfer (FRET) measurements at the single-molecule level.

317
318 Readout is not limited to single-particle fluorescence burst detection. As proof of concept, we also explored other
319 fluorescence microscopy techniques (confocal imaging and TIRF microscopy) as alternative readout techniques
320 to be used in combination with nanofluidics (**S4, S5**). This gives laboratories guidance on how to use nano-trapping
321 devices with their already available fluorescence microscopy equipment according to their needs and research
322 applications. This highlights the versatility of the applications that can be envisaged with our nanofluidic device
323 in conjunction with different optical modalities. We anticipate that the cost-effective and easy approach for
324 fabrication of nanofluidic devices has the potential to find broad applicability in various applications in the
325 nanobiotechnologies, biophysics, and clinical diagnostics. Researchers interested in topics such as synthesis and
326 functionalization of nanoparticles for nanomedicine and drug delivery [46], metal-organic frameworks [47], guest-
327 host complexes [48], carbon quantum dots [49], bottom-up assembled meta materials (e.g. gold nano cubes, gold
328 nanoparticles) [7], active colloids [50] (e.g., Janus particles) or general spectroscopic analysis of light-matter
329 interactions in solution [51] (e.g., Raman spectroscopy, second-harmonic generation (SHG), non-linear refractive
330 indices, FRET), would greatly benefit from the approach presented here.

331
332 Similar nanofluidic devices were previously established by Krishnan et al. for the geometry-induced electrostatic
333 trapping of nano-colloids[22], where iSCAT provided a label-free readout method of gold nanoparticle and
334 liposome residence times in the nanoconfinement. The silica-based devices were fabricated using RIE etching and
335 involved several clean room fabrication steps - therefore are not easily prototyped by biological laboratories with
336 limited access to nanofabrication facilities. An important step to make this technology more available to the
337 research community was achieved by Gerspach et al. [52] who moulded electrostatic trapping devices in PDMS
338 and measured the residence time of highly charged gold nanoparticles of 60 nm, 80 nm and 100 nm diameter in
339 nano-pockets. Their experiments showed that confinement is highly dependent of the size ratio between the particle
340 and the trap, which underlines the importance of flexible fabrication schemes that can adapt to the application
341 accordingly.

342
343 By contrast, the method demonstrated in the present paper shows the advantage of a stationary chip design without
344 external machinery to study a variety of biological specimen from colloids to oligomers and DNA molecules in
345 confined space, without permanently immobilizing or perturbing these. EBL and RIE as the golden standards for
346 the fabrication of silica trapping devices have higher lateral resolution than 2PL, but 2PL allows a more versatile
347 integration of complex nanofluidic and nano-trapping geometries into microfluidic device platforms in the sub-
348 micron regime.

349
350 Taken together, in this paper, we give a cost-effective and facile approach for the fabrication of nanofluidic devices
351 to study single molecules in solution without permanent surface immobilization using hybrid 2-photon
352 lithography. With our approach we envisage to facilitate nanoparticle trapping technology in biological and

353 biomedical laboratories, paving the way for the use of photon-intensive spectroscopic techniques for applications
354 related to protein misfolding disease, cancer research, and bionanotechnology.

355

356 Methods

357

358 Wafer preparation and development

360 SU-8 photoresist (Type 3025, Micro Resist Technology) was spin coated (Laurell technologies, WS-650) at
361 3000 rpm onto a 3-inch silicon wafer (MicroChemicals, Prime CZ-Si, thickness 381 +/- 20 µm, polished, p-type)
362 to a height of 25 µm. The SU-8 coated wafer was soft baked and treated according to the protocol of the supplier
363 of the photoresist. Microfluidic patterns from a custom-designed film mask (Microlithography) were then
364 projected onto the wafer and the photoresist was exposed for 30 seconds with the UV-LED setup as described in
365 Challa et al. [53]. The wafer was post baked at 95 °C so that the interfaces between exposed and unexposed regions
366 become visible due to their change in refractive index, which assisted in alignment of the microstructures with the
367 2PL setup. After the nanostructures were written with 2PL and the wafer baked at 95 °C for 8 minutes. The wafer
368 was developed using Propylene-glycol-monomethyl-ether-acetate (PGMEA) (Sigma-Aldrich) and subsequently
369 given a second exposure with UV light for 30 seconds to make structures mechanically stable on the wafer before
370 final rinsing of the structures with PGMEA and Isopropanol (IPA) (Sigma-Aldrich) [39]. A post-bake of 30
371 minutes at 95 °C on a hot plate was done at the end of the development process to increase mechanical stability of
372 the nanostructures.

373

374 2-photon lithography

375 A custom-built 2PL setup was used to write the calibration patterns as well as the final nanofluidic master mould.
376 A detailed description of the upright 2-photon lithography setup and its fabrication capabilities can be found in
377 Vanderpoorten et al. [32]. Briefly, the system uses a femto-second fibre laser (Menlo System C Fiber 780 HP)
378 modulated as the first diffraction order of an acousto-optic modulator (AA Optoelectronics). The beam is widened
379 through a beam expander (Thorlabs, BE02-05-B) and led over a 90:10 R:T beamsplitter (BS028, Thorlabs) into a
380 microscope objective vertically mounted above the sample. Reflected light is collected with a tube lens (Thorlabs
381 AC 254-100-A-ML, BBAR coating A OM 31 400–700 nm, f = 100.0 mm) onto a camera (μ Eye ML, Industry
382 camera, USB 3.0). An optical electro-mechanical shutter (Thorlabs, SHB1) is mounted in front of the camera to
383 protect it during high power laser writing. Through an additional 30:70 (R:T) beam splitter (BS019, Thorlabs) in
384 the camera detection arm, a white LED (Thorlabs, MCWHL5) allows non-polymerizing inspection of the sample
385 in wide field. A 3-inch wafer coated with pre-baked SU-8 (25 µm thickness) was immobilised on a PI Nanocube
386 (P-611.3S, Physikalische Instrumente) mounted on two perpendicular stacked motorised linear-precision stages
387 (M-404.2PD, Physikalische Instrumente, Ball screw, 80 mm wide, ActiveDrive). Immersion Oil (Cargille
388 laboratories, LDF, Code 387) was added onto the SU-8 layer before bringing the oil immersion objective (Leica,
389 63x, PL APO, 1.40 NA) manually in close proximity to the wafer surface. The oil used here showed no reaction
390 with unpolymerised SU-8 photo resin and facilitates easy and scalable two-photon printing. Custom-written
391 software then automatically focusses on the wafer surface, corrects for tilt and coordinates the interplay of piezo,
392 translational stages and laser power modulation to write the intended patterns. The laser beam intensity of the
393 writing beam was directly measured after the acousto-optic modulator using a power meter (Thorlabs, S310C,
394 thermal power head). To prevent exposure of the resin during the focussing process, the laser power was kept
395 below the polymerization threshold, but high enough to be detected on the system's camera. The full travel range
396 of the Nanocube of 100 µm x 100 µm was used to write a calibration array of lines and dots. Then the motorized
397 stages were used to displace the piezo scanning areas and write a new pattern (e.g., 300 µm displacement,
398 positional precision = 1 µm) with adapted parameters. The positioning repeatability of the piezo actor (Nanocube)
399 was below 10 nm according of the manufacturer and is key for automated focussing and reliable nanofabrication.
400 For 2-photon-writing in the microfluidic master, we used a white light LED to first place the laser focus in between
401 the two micro-channels and then started the automated laser writing process. The system uses the autofocus
402 function each time it adds another nanofluidic array. This allows step wise but precise addition of nanofluidic
403 features on the wafer scale.

404

406 **Correlative scanning electron microscopy and atomic force microscopy imaging**

407
408 After the development process of the 2-photon written calibration assay, the wafer was manually cut into smaller
409 dimensions to allow easier sample handling. Imprints of the master wafer were taken following conventional soft
410 lithography protocols PDMS (Sylgard 184) with 10:1 curing agent ratio. After PDMS curation, the area of interest
411 was cut out using a surgical scalpel. The PDMS imprint was coated with 10 nm platinum (Quorum Technologies
412 Q150T ES Turbo-Pumped Sputter Coater/Carbon Coater) and imaged using a commercial SEM (TESCAN
413 MIRA3 FEG-SEM). The original SU-8 features were coated with a layer of 10 nm platinum as well and imaged
414 on the same SEM in order to compare the imprinted features with the original moulds. The final nanofluidic PDMS
415 device imprint was imaged following the same procedures and imaged on the same microscope. AFM was
416 conducted on the calibration sample using a Park Systems NX10 AFM. According to previous findings by Cabrera
417 et al. [54] the PDMS surface roughness can be assumed to be below 5 nm, which should therefore not influence
418 the steric trapping behaviour significantly.

419
420 **Profilometer measurements of nano-traps**

421
422 The 2-photon written nanofluidic master wafer was cleaned using pressurised air and placed in a profilometer
423 (KLA Corporation, Tencor P-6) for height measurements of nano-channels and nano-traps. Using the integrated
424 microscope of the system, the scan direction was aligned along the centre of a nano-trapping array located between
425 the two microfluidic reservoirs. The sample was scanned at a speed of 2.00 $\mu\text{m}/\text{s}$, with a height scan rate of 500
426 Hz and a force of 0.5 mg applied using a 2.00 μm (diameter) tip.

427
428 **Single-molecule confocal measurements**

429
430 Single-molecule fluorescence measurements were performed on a custom-built single-molecule confocal
431 microscope. Nanofluidic PDMS–silica devices were secured to a motorised microscope stage (Applied Scientific
432 Instrumentation, PZ-2000FT). The sample was excited using a 488 nm wavelength laser (Cobolt 06-MLD, 200
433 mW diode laser, Cobolt), which was directed to the back aperture of a 60X-magnification water-immersion
434 objective (CFI Plan Apochromat WI 60x, NA 1.2, Nikon) using a single-mode optical fibre (P3-488PM-FC-1,
435 Thorlabs) and an achromatic fibre collimator (60FC-L-4-M100S-26, Schäfter/Kirchhoff GmbH). The laser
436 intensity at the back aperture of the objective was adjusted to 150 μW . The laser beam exiting the optical fibre
437 was reflected by a dichroic mirror (Di03-R488/561, Semrock), directed to the objective and focussed into the chip
438 to a diffraction-limited confocal spot. The motorised stage was used to position the confocal spot within the chip.
439 The emitted light from the sample was collected through the same objective and dichroic mirror and then passed
440 through a 30 μm pinhole (Thorlabs) to remove any out-of-focus light. The emitted photons were filtered through
441 a band-pass filter (FF01-520/35-25, Semrock) and then focussed onto an avalanche photodiode (APD, SPCM-14,
442 PerkinElmer Optoelectronics) connected to a TimeHarp260 time-correlated single-photon counting unit
443 (PicoQuant). Photon time traces were recorded using the SymPhoTime 64 software package (Picoquant) with a
444 binning time of 1 ms.

445
446 **Preparation of labelled α -synuclein oligomers**

447
448 The N122C variant of α -synuclein was purified into phosphate buffered saline (PBS) pH 7.4 as described
449 previously [55], with the addition of 3 mM DTT to all buffers to prevent dimerization. Following removal of DTT
450 from the purified monomers by a PD10 desalting column packed with Sephadex G25 matrix (GE Healthcare), the
451 protein was incubated with a 1.5-fold molar excess of Alexa488 with a maleimide linker (ThermoFisher Scientific)
452 (overnight, 4 °C on a rolling system). In order to remove the free dye, the mixture was subsequently subjected to
453 size exclusion chromatography using a Superdex 200 16/600 (GE Healthcare) and eluted in PBS pH 7.4 at 20 °C.
454 Protein fractions were pooled, and Alexa488 labelled α -synuclein concentration estimated by dye absorbance,
455 assuming 1:1 dye:protein stoichiometry (72 000 L/mol cm at 495 nm). Stable α -synuclein oligomers were formed
456 from Alexa488 labelled monomers, as previously described [56]. Briefly, monomeric α -synuclein was lyophilised
457 in Milli-Q water and resuspended in PBS pH 7.4 at a concentration of 12 mg/m. Following incubation (37 °C, 20–
458 24 h), the samples were ultracentrifuged (1h, 288'000 x g) (Optima TLX Ultracentrifuge, Beckman Coulter, TLA-

459 120.2 Beckman rotor) to remove large aggregates. Monomeric protein was removed by multiple filtration steps
460 through 100 kDa concentrating filters. The oligomer concentration was estimated based on the dye absorbance
461 (72'000 L/mol cm at 495 nm).

462

463 Sample and device preparation for single molecule experiments

464

465 100 nm and 40 nm fluorescent colloids (FluoSpheres) were purchased from ThermoFisher. α -synuclein oligomers
466 were prepared as described above. Double-stranded DNA was prepared from two single-stranded DNA
467 oligonucleotides by thermal annealing. Oligonucleotides were synthesized and labelled by Biomers. The
468 sequences were: 5'-GCC TTA TTT TCA CTC TTT CCT TTC TTC TCT CTT TTT TTC CCG-3' (top strand)
469 and 5'-CGG GAA AAA AAG AGA GAA GAA AGG AAA GAG TGA AAA TAA GGC-3' (bottom strand);
470 the top strand was labelled with Atto488 at the thymidine at position 7, shown in bold type.

471 Micro-/nanofluidic devices were moulded from the fabricated SU-8 master via soft lithography using PDMS
472 (Sylgard 184; with 10:1 curing agent ratio). After baking, inlets were added using surgical punchers and plasma
473 bonded to coverslip glasses (Menzel coverslips, Grade H1.5). The surface of the coverslips and the PDMS were
474 plasma treated, and afterwards manually pressed on top of each other. Devices were used directly after the plasma
475 bonding step to use their remaining surface hydrophilicity for easier filling of the devices. Before the experiments,
476 the chips were filled by pipetting equal amounts of diluted sample solutions into the inlet areas and equilibrated
477 for 20 minutes.

478

479 Supporting information

480

481 Additional surface structure analysis and image data acquired by AFM on 2p-fabricated nano-trap master wafer
482 (SU-8 on silicon); profilometer data of master wafer used for confocal fluorescence burst detection experiments;
483 comparative figure of fluorescence burst traces of 100 nm colloids, oligomers and 40 bp DNA; experimental
484 description of confocal microscopy and TIRF imaging for 100nm and 40 nm particle detection in nano-traps;
485 images, kymographs and traces acquired using former mentioned fluorescence microscopy imaging techniques

486

487 Bibliography

488

- 489 [1] D. Gao, W. Ding, M. Nieto-Vesperinas, X. Ding, M. Rahman, T. Zhang, C. Lim & CW. Qiu , “Optical
490 manipulation from the microscale to the nanoscale: fundamentals, advances and prospects,” *Light Sci.
491 Appl.*, vol. 6, no. 9, pp. e17039–e17039, 2017, doi: 10.1038/lsci.2017.39.
- 492 [2] Q. Wang, R. H. Goldsmith, Y. Jiang, S. D. Bockenhauer, and W. E. Moerner, “Probing single biomolecules
493 in solution using the anti-brownian electrokinetic (ABEL) trap,” *Acc. Chem. Res.*, vol. 45, no. 11, pp. 1955–
494 1964, Nov. 2012, doi: 10.1021/ar200304t.
- 495 [3] T. Huang and C.-X. Deng, “Current Progresses of Exosomes as Cancer Diagnostic and Prognostic
496 Biomarkers,” *Int. J. Biol. Sci.*, vol. 15, no. 1, pp. 1–11, Jan. 2019, doi: 10.7150/ijbs.27796.
- 497 [4] A. H. Squires, P. D. Dahlberg, H. Liu, N. C. M. Magdaong, R. E. Blankenship, and W. E. Moerner, “Single-
498 molecule trapping and spectroscopy reveals photophysical heterogeneity of phycobilisomes quenched by
499 Orange Carotenoid Protein,” *Nat. Commun.*, vol. 10, no. 1, pp. 1–12, Dec. 2019, doi: 10.1038/s41467-019-
500 09084-2.
- 501 [5] A. H. Squires, A. A. Lavania, P. D. Dahlberg, and W. E. Moerner, “Interferometric Scattering Enables
502 Fluorescence-Free Electrokinetic Trapping of Single Nanoparticles in Free Solution,” *Nano Lett.*, vol. 19,
503 no. 6, pp. 4112–4117, Jun. 2019, doi: 10.1021/acs.nanolett.9b01514.
- 504 [6] A. E. Cohen and W. E. Moerner, “Method for trapping and manipulating nanoscale objects in solution,”
505 *Appl. Phys. Lett.*, vol. 86, no. 9, pp. 1–3, Feb. 2005, doi: 10.1063/1.1872220.
- 506 [7] M. E. Mann, P. Yadav, and S. Kim, “Colloidal Plasmonic Nanocubes as Capacitor Building Blocks for
507 Multidimensional Optical Metamaterials: A Review,” *ACS Appl. Nano Mater.*, vol. 4, no. 10, pp. 9976–

- 509 9984, Oct. 2021, doi: 10.1021/ACSANM.1C02211.
- 510 [8] P. C. Ke, R. Zhou, L. C. Serpell, R. Riek, T. P. J. Knowles, H. A. Lashuel, E. Gazit, I. W. Hamley, T. P.
511 Davis, M. Fändrich, D. E. Otzen, M. R. Chapman, C. M. Dobson, D. S. Eisenberg and R. Mezzenga , “Half
512 a century of amyloids: past, present and future,” *Chem. Soc. Rev.*, vol. 49, no. 15, pp. 5473–5509, Aug.
513 2020, doi: 10.1039/C9CS00199A.
- 514 [9] M. Endo, Y. Yang, and H. Sugiyama, “Biomaterials Science REVIEW DNA origami technology for
515 biomaterials applications,” 2013, doi: 10.1039/c2bm00154c.
- 516 [10] M. Barzegar Amiri Olia, P. S. Donnelly, L. C. L. Hollenberg, P. Mulvaney, and D. A. Simpson, “Advances
517 in the Surface Functionalization of Nanodiamonds for Biological Applications: A Review,” *ACS Appl.
518 Nano Mater.*, vol. 4, no. 10, pp. 9985–10005, Oct. 2021, doi: 10.1021/ACSANM.1C02698.
- 519 [11] R. Roy, S. Hohng, and T. Ha, “A practical guide to single-molecule FRET,” *Nature Methods*, vol. 5, no. 6.
520 NIH Public Access, pp. 507–516, Jun. 2008, doi: 10.1038/nmeth.1208.
- 521 [12] L. Grasso, R. Wyss, L. Weidenauer, A. Thampi, D. Demurtas, M. Prudent, N. Lion & H. Vogel , “Molecular
522 screening of cancer-derived exosomes by surface plasmon resonance spectroscopy.,” *Anal. Bioanal.
523 Chem.*, vol. 407, no. 18, pp. 5425–5432, Jul. 2015, doi: 10.1007/s00216-015-8711-5.
- 524 [13] U. B. Choi, K. R. Weninger, and M. E. Bowen, “Immobilization of proteins for single-molecule
525 fluorescence resonance energy transfer measurements of conformation and dynamics,” *Methods Mol. Biol.*,
526 vol. 896, pp. 3–20, 2012, doi: 10.1007/978-1-4614-3704-8_1.
- 527 [14] H. Y. Yang and W. E. Moerner, “Resolving Mixtures in Solution by Single-Molecule Rotational
528 Diffusivity,” *Nano Lett.*, vol. 18, no. 8, pp. 5279–5287, Aug. 2018, doi: 10.1021/acs.nanolett.8b02280.
- 529 [15] M. Tanyeri and C. M. Schroeder, “Manipulation and Confinement of Single Particles Using Fluid Flow,”
530 *Nano Lett.*, vol. 13, no. 6, pp. 2357–2364, Jun. 2013, doi: 10.1021/nl4008437.
- 531 [16] C. Bradac, “Nanoscale Optical Trapping: A Review,” *Adv. Opt. Mater.*, vol. 6, no. 12, p. 1800005, Jun.
532 2018, doi: 10.1002/adom.201800005.
- 533 [17] C. Chen, M. L. Juan, Y. Li, G. Maes, G. Borghs, P. Van Dorpe, R. Quidant, “Enhanced optical trapping
534 and arrangement of nano-objects in a plasmonic nanocavity,” *Nano Lett.*, vol. 12, no. 1, pp. 125–132, Jan.
535 2012, doi: 10.1021/nl2031458.
- 536 [18] J. E. Melzer and E. McLeod, “Fundamental Limits of Optical Tweezer Nanoparticle Manipulation Speeds,”
537 *ACS Nano*, vol. 12, no. 3, pp. 2440–2447, Mar. 2018, doi: 10.1021/acsnano.7b07914.
- 538 [19] E. H. Hill, J. Li, L. Lin, Y. Liu, and Y. Zheng, “Opto-Thermophoretic Attraction, Trapping, and Dynamic
539 Manipulation of Lipid Vesicles,” *Langmuir*, vol. 34, no. 44, pp. 13252–13262, Nov. 2018, doi:
540 10.1021/acs.langmuir.8b01979.
- 541 [20] J. Chen, H. Cong, F.C. Loo, Z. Kang, M. Tang, H. Zhang, SY. Wu, SK. Kong & HP. Ho , “Thermal gradient
542 induced tweezers for the manipulation of particles and cells.,” *Sci. Rep.*, vol. 6, p. 35814, Nov. 2016, doi:
543 10.1038/srep35814.
- 544 [21] K. Wang, E. Schonbrun, P. Steinurzel, and K. B. Crozier, “Trapping and rotating nanoparticles using a
545 plasmonic nano-tweezer with an integrated heat sink,” *Nat. Commun.*, vol. 2, no. 1, p. 469, 2011, doi:
546 10.1038/ncomms1480.
- 547 [22] M. Krishnan, N. Mojarrad, P. Kukura, and V. Sandoghdar, “Geometry-induced electrostatic trapping of
548 nanometric objects in a fluid,” *Nature*, vol. 467, no. 7316, pp. 692–695, 2010, doi: 10.1038/nature09404.
- 549 [23] M. Krishnan, “Electrostatic free energy for a confined nanoscale object in a fluid,” *J. Chem. Phys.*, vol.
550 138, no. 11, p. 114906, Mar. 2013, doi: 10.1063/1.4795087.
- 551 [24] M. I. Bespalova, S. Mahanta, and M. Krishnan, “Single-molecule trapping and measurement in solution,”
552 *Curr. Opin. Chem. Biol.*, vol. 51, pp. 113–121, 2019, doi: 10.1016/j.cbpa.2019.05.013.
- 553 [25] N. Mojarrad and M. Krishnan, “Measuring the size and charge of single nanoscale objects in solution using

- 554 an electrostatic fluidic trap," *Nat. Nanotechnol.*, vol. 7, no. 7, pp. 448–452, 2012, doi:
555 10.1038/nnano.2012.99.
- 556 [26] F. Ruggeri and M. Krishnan, "Entropic Trapping of a Singly Charged Molecule in Solution," *Nano Lett.*,
557 vol. 18, no. 6, pp. 3773–3779, Jun. 2018, doi: 10.1021/acs.nanolett.8b01011.
- 558 [27] F. Ruggeri, F. Zosel, N. Mutter, M. Rózycka, M. Wojtas, A. Ozyhar, B. Schuler & M. Krishnan , "Single-
559 molecule electrometry," *Nat. Nanotechnol.*, vol. 12, no. 5, pp. 488–495, 2017, doi: 10.1038/nnano.2017.26.
- 560 [28] C. Duan, W. Wang, and Q. Xie, "Review article: Fabrication of nanofluidic devices," *Biomicrofluidics*,
561 vol. 7, no. 2, p. 26501, Mar. 2013, doi: 10.1063/1.4794973.
- 562 [29] L. D. Menard and J. M. Ramsey, "Electrokinetically-driven transport of DNA through focused ion beam
563 milled nanofluidic channels.,," *Anal. Chem.*, vol. 85, no. 2, pp. 1146–1153, Jan. 2013, doi:
564 10.1021/ac303074f.
- 565 [30] G. Bruno, N. D. Trani, R. L. Hood, E. Zabre, C. S. Filgueira, G. Canavese, P. Jain, Z. Smith, D. Demarchi,
566 S. Hosali, A. Pimpinelli, M. Ferrari & A. Grattoni , "Unexpected behaviors in molecular transport through
567 size-controlled nanochannels down to the ultra-nanoscale," *Nat. Commun.*, vol. 9, no. 1, pp. 1–10, 2018,
568 doi: 10.1038/s41467-018-04133-8.
- 569 [31] S. Maruo, O. Nakamura, and S. Kawata, "Three-dimensional microfabrication with two-photon-absorbed
570 photopolymerization," *Opt. Lett.*, vol. 22, no. 2, p. 132, Jan. 1997, doi: 10.1364/OL.22.000132.
- 571 [32] O. Vanderpoorten, Q. Peter, P. K. Challa, U. F. Keyser, J. J. Baumberg, C. F. Kaminski & T. P. J. Knowles
572 , "Scalable integration of nano-, and microfluidics with hybrid two-photon lithography," *Microsystems
573 Nanoeng.*, vol. 5, no. 1, pp. 1–9, Dec. 2019, doi: 10.1038/s41378-019-0080-3.
- 574 [33] C. Barner-Kowollik, M. Bastmeyer, E. Blasco, G. Delaittre, P. Müller, B. Richter, M. Wegener , "3D Laser
575 Micro- and Nanoprinting: Challenges for Chemistry," *Angewandte Chemie - International Edition*, vol. 56,
576 no. 50. Wiley-VCH Verlag, pp. 15828–15845, Dec. 11, 2017, doi: 10.1002/anie.201704695.
- 577 [34] X. Zhou, Y. Hou, and J. Lin, "A review on the processing accuracy of two-photon polymerization," *AIP
578 Adv.*, vol. 5, no. 3, p. 30701, Mar. 2015, doi: 10.1063/1.4916886.
- 579 [35] M. Oellers, F. Lucklum, and M. J. Vellekoop, "On-chip mixing of liquids with swap structures written by
580 two-photon polymerization," *Microfluid. Nanofluidics*, vol. 24, no. 1, p. 4, Jan. 2020, doi: 10.1007/s10404-
581 019-2309-8.
- 582 [36] K. Venkatakrishnan, S. Jariwala, and B. Tan, "Maskless fabrication of nano-fluidic channels by two-photon
583 absorption (TPA) polymerization of SU-8 on glass substrate," *Opt. Express*, vol. 17, no. 4, p. 2756, Feb.
584 2009, doi: 10.1364/oe.17.002756.
- 585 [37] K. Sugioka, J. Xu, D. Wu, Y. Hanada, Z. Wang, Y. Cheng, K. Midorikawa , "Femtosecond laser 3D
586 micromachining: A powerful tool for the fabrication of microfluidic, optofluidic, and electrofluidic devices
587 based on glass," *Lab on a Chip*, vol. 14, no. 18. Royal Society of Chemistry, pp. 3447–3458, Sep. 21, 2014,
588 doi: 10.1039/c4lc00548a.
- 589 [38] Y. Xia and G. M. Whitesides, "Soft lithography," *Annu. Rev. Mater. Sci.*, vol. 28, 1998, doi:
590 10.1146/annurev.matsci.28.1.153.
- 591 [39] J. Purto, A. Verch, P. Rogin, and R. Hensel, "Improved development procedure to enhance the stability
592 of microstructures created by two-photon polymerization," *Microelectron. Eng.*, vol. 194, pp. 45–50, Jul.
593 2018, doi: 10.1016/j.mee.2018.03.009.
- 594 [40] G. M. Whitesides, "The origins and the future of microfluidics," *Nature*, vol. 442, no. 7101. Nature
595 Publishing Group, pp. 368–373, Jul. 27, 2006, doi: 10.1038/nature05058.
- 596 [41] A. M. Streets and Y. Huang, "Microfluidics for biological measurements with single-molecule resolution,"
597 *Current Opinion in Biotechnology*, vol. 25. Elsevier Current Trends, pp. 69–77, Feb. 01, 2014, doi:
598 10.1016/j.copbio.2013.08.013.

- 599 [42] R. M. Guijt and A. Manz, "Miniaturised total chemical-analysis systems (MTAS) that periodically convert
600 chemical into electronic information," *Sensors and Actuators, B: Chemical*, vol. 273. Elsevier B.V., pp.
601 1334–1345, Nov. 10, 2018, doi: 10.1016/j.snb.2018.06.054.
- 602 [43] C. E. Castro, F. Kilchherr, DN. Kim, E. L. Shiao, T. Wauer, P. Wortmann, M. Bathe, H. Dietz , "A primer
603 to scaffolded DNA origami," *Nat. Methods*, vol. 8, no. 3, pp. 221–229, Mar. 2011, doi:
604 10.1038/nmeth.1570.
- 605 [44] S. Guilbaud, L. Salomé, N. Destainville, M. Manghi, and C. Tardin, "Dependence of DNA Persistence
606 Length on Ionic Strength and Ion Type," *Phys. Rev. Lett.*, vol. 122, no. 2, p. 028102, Jan. 2019, doi:
607 10.1103/PhysRevLett.122.028102.
- 608 [45] R. B. Schoch, J. Han, and P. Renaud, "Transport phenomena in nanofluidics," *Rev. Mod. Phys.*, vol. 80,
609 2008, doi: 10.1103/RevModPhys.80.839.
- 610 [46] Tennyson L. Doane and Clemens Burda, "The unique role of nanoparticles in nanomedicine: imaging, drug
611 delivery and therapy," *Chem. Soc. Rev.*, vol. 41, no. 7, pp. 2885–2911, Mar. 2012, doi:
612 10.1039/C2CS15260F.
- 613 [47] W. L. Jhang, M. S. Huang, and S. W. Hsu, "Unsymmetrical Heterogeneous Au-Ag Nanocrystals as
614 Catalysts, Sensors, and Drug Carriers," *ACS Appl. Nano Mater.*, vol. 4, no. 10, pp. 10011–10017, Oct.
615 2021, doi: 10.1021/ACSANM.1C02866/SUPPL_FILE/AN1C02866_SI_001.PDF.
- 616 [48] T. Xiong, Y. Zhang, L. Donà, M. Gutiérrez, A. F. Mösllein, Az.S. Babal, N.Amin, B. Civalleri, and JC.
617 Tan, "Tunable Fluorescein-Encapsulated Zeolitic Imidazolate Framework-8 Nanoparticles for Solid-State
618 Lighting," *ACS Appl. Nano Mater.*, vol. 4, no. 10, pp. 10321–10333, Oct. 2021, doi:
619 10.1021/ACSANM.1C01829/SUPPL_FILE/AN1C01829_SI_002.PDF.
- 620 [49] S. Y. Lim, W. Shen, and Z. Gao, "Carbon quantum dots and their applications," *Chem. Soc. Rev.*, vol. 44,
621 no. 1, pp. 362–381, Dec. 2014, doi: 10.1039/C4CS00269E.
- 622 [50] Z. Wang, Z. Wang, J. Li, C. Tian, and Y. Wang, "Active colloidal molecules assembled via selective and
623 directional bonds," *Nat. Commun.* 2020 111, vol. 11, no. 1, pp. 1–12, May 2020, doi: 10.1038/s41467-020-
624 16506-z.
- 625 [51] TC. Huang, HC. Tsai, YC. Chin, WS. Huang, YC. Chiu, TC. Hsu, ZC. Chia, TC. Hung, CC. Huang, and
626 YT. Hsieh , "Concave Double-Walled AgAuPd Nanocubes for Surface-Enhanced Raman Spectroscopy
627 Detection and Catalysis Applications," *ACS Appl. Nano Mater.*, vol. 4, no. 10, pp. 10103–10115, Oct.
628 2021, doi: 10.1021/ACSANM.1C01534/SUPPL_FILE/AN1C01534_SI_001.PDF.
- 629 [52] M. A. Gerspach, N. Mojarrad, D. Sharma, T. Pfohl, and Y. Ekinci, "Soft electrostatic trapping in
630 nanofluidics," *Microsystems Nanoeng.*, vol. 3, no. 1, p. 17051, 2017, doi: 10.1038/micronano.2017.51.
- 631 [53] P. K. Challa, T. Kartanas, J. Charmet, and T. P. J. Knowles, "Microfluidic devices fabricated using fast
632 wafer-scale LED-lithography patterning," *Biomicrofluidics*, vol. 11, 2017, doi: 10.1063/1.4976690.
- 633 [54] J. N. Cabrera, M. M. Ruiz, M. Fascio, N. D'Accorso, R. Mincheva, P. Dubois, L. Lizarraga, and R. M.
634 Negri , "Increased Surface Roughness in Polydimethylsiloxane Films by Physical and Chemical Methods,"
635 *Polymers (Basel)*., vol. 9, no. 8, p. 331, Aug. 2017, doi: 10.3390/POLYM9080331.
- 636 [55] W. Hoyer, T. Antony, D. Cherny, G. Heim, T. M. Jovin, and V. Subramaniam, "Dependence of α -synuclein
637 aggregate morphology on solution conditions," *J. Mol. Biol.*, vol. 322, no. 2, pp. 383–393, Sep. 2002, doi:
638 10.1016/S0022-2836(02)00775-1.
- 639 [56] S. W. Chen , S. Drakulic, E. Deas, M. Ouberai, F. A. Aprile, R. Arranz, S. Ness, C. Roodveldt, T. Guilliams,
640 E. J. De-Genst, D. Klenerman, N. W. Wood, T. P. J. Knowles, C. Alfonso, G. Rivas, A. Y. Abramov, J. M.
641 Valpuesta, C. M. Dobson, N. Cremades, "Structural characterization of toxic oligomers that are kinetically
642 trapped during α -synuclein fibril formation," *Proc. Natl. Acad. Sci. U. S. A.*, vol. 112, no. 16, pp. E1994–
643 E2003, Apr. 2015, doi: 10.1073/pnas.1421204112.

645 **Acknowledgements**

646
647 The work was funded by the Horizon 2020 programme through 766972-FET-OPEN-NANOPHLOW (TPJK). The
648 research leading to these results has further received funding from the European Research Council under the
649 European Union's Horizon 2020 Framework Programme through the Marie Skłodowska-Curie grant
650 MicroSPARK (agreement n° 841466; GK), the Herchel Smith Funds (GK), and the Wolfson College Junior
651 Research Fellowship (G.K.). This work was also supported by the Engineering and Physical Sciences Research
652 Council [grant numbers EP/L015889/1]. The authors would also like to thank the NanoDTC for additional funding
653 and the Maxwell Community for scientific support.

654
655 **Author contributions statement**

656
657 OV and ANB fabricated nanofluidic masters and chips using two-photon lithography. ANB characterised the
658 calibration assays using SEM and AFM. OV conducted profilometer measurements on nanofluidic master wafer.
659 GK built the confocal burst detection setup and conducted the fluorescence burst experiments of colloids,
660 oligomers, and DNA in nano-trap devices and micro-channels. OV and ANB imaged trapping events of colloidal
661 particles using confocal microscopy. PKC, ZT, ANB and OV conducted TIRF microscopy measurements of
662 colloidal particles. PKC and ZT also conducted trapping experiments using conventional UV-lithography in an
663 early stage of the project, which helped form the content of this paper. RJ contributed with data analysis and wrote
664 software for the residence time measurements of the fluorescence burst data. QP improved the control software of
665 the two-photon system which allowed initial test runs and to conduct the fabrication assay. CX prepared and
666 purified oligomer samples used for all the experiments. OV, GK, and ANB wrote the paper. All authors provided
667 input into the manuscript.